

CHEMISTRY

AN ASIAN JOURNAL

www.chemasianj.org

Accepted Article

Title: A general strategy for the construction of NIR emitting Si-rhodamines and their application for mitochondrial temperature visualization

Authors: Weiguo Tang, Han Gao, Jiaxin Li, Xianhui Wang, Zhikuan Zhou, Lizhi Gai, Xin Jiang Feng, Jiangwei Tian, Hua Lu, and Zijian Guo

This manuscript has been accepted after peer review and appears as an Accepted Article online prior to editing, proofing, and formal publication of the final Version of Record (VoR). This work is currently citable by using the Digital Object Identifier (DOI) given below. The VoR will be published online in Early View as soon as possible and may be different to this Accepted Article as a result of editing. Readers should obtain the VoR from the journal website shown below when it is published to ensure accuracy of information. The authors are responsible for the content of this Accepted Article.

To be cited as: *Chem. Asian J.* 10.1002/asia.202000660

Link to VoR: <https://doi.org/10.1002/asia.202000660>

A Journal of



A sister journal of *Angewandte Chemie*
and *Chemistry – A European Journal*

WILEY-VCH

FULL
PAPER

A general strategy for the construction of NIR emitting Si-rhodamines and their application for mitochondrial temperature visualization

Weiguo Tang,[†] [a] Han Gao,[†] [b] Jiaxin Li,^[a] Xianhui Wang,^[a] Zhikuan Zhou,^[a] Lizhi Gai,^[a] Xin Jiang Feng,^{*[a]} Jiangwei Tian,^{*[b]} Hua Lu,^{*[a]} and Zijian Guo^{*[c]}

[a] W. Tang, J. Li, X. Wang, Dr. Z. Zhou, Dr. L. Gai, Dr. X. Feng, Prof. Dr. H. Lu, Key Laboratory of Organosilicon Chemistry and Material Technology of Ministry of Education, and Key Laboratory of Organosilicon Material of Zhejiang Province, Hangzhou Normal University, No. 2318, Yuhangtang Road, Hangzhou 311121, P. R. China. E-mail: xjfeng@hznu.edu.cn; hualu@hznu.edu.cn

[b] H. Gai, Dr. J. Tian, State Key Laboratory of Natural Medicines, Jiangsu Key Laboratory of TCM Evaluation and Translational Research, China Pharmaceutical University, Nanjing 211198, China. Email: jwitian@cpu.edu.cn

[c] Prof. Dr. Z. Guo, State Key Laboratory of Coordination Chemistry, School of Chemistry and Chemical Engineering, Nanjing University, Nanjing, 210023, P. R. China. E-mail: zguo@nju.edu.cn

Supporting information for this article is given via a link at the end of the document.

Abstract: Si-rhodamine (SiR) is an ideal fluorophore because it possesses bright emitting in the NIR region and can be implemented flexibly in living cell. Currently, several promising approaches for synthesizing SiR are being developed. However, challenges remain in the construction of SiR containing functional groups for bioimaging application. Herein, we introduce a general and simple approach by a condensation reaction of diarylsilyl ether and arylaldehyde in *o*-dichlorobenzene to synthesize a series of SiRs bearing various functional substituents. These SiRs have moderate to high quantum efficiency, tolerance to photobleaching, and high water solubility as well as NIR emitting, and their NIR fluorescence properties can be controlled through the photoinduced electron transfer (PET) mechanism. Fluorescence OFF-ON switching effect is observed for SiR **9** in the presence of acid, which is rationalized by DFT/TDDFT calculations. Moreover, reversible stimuli response toward temperature is achieved. Since positive charge enables mitochondrial targeting ability and chloromethyl unit can covalently immobilize the dyes onto the mitochondrial via click reaction between the benzyl chloride and protein sulfhydryls, SiR **8** is identified as a valuable fluorescent marker to visualize the morphology and monitor the temperature change of mitochondrial with high photostability.

Introduction

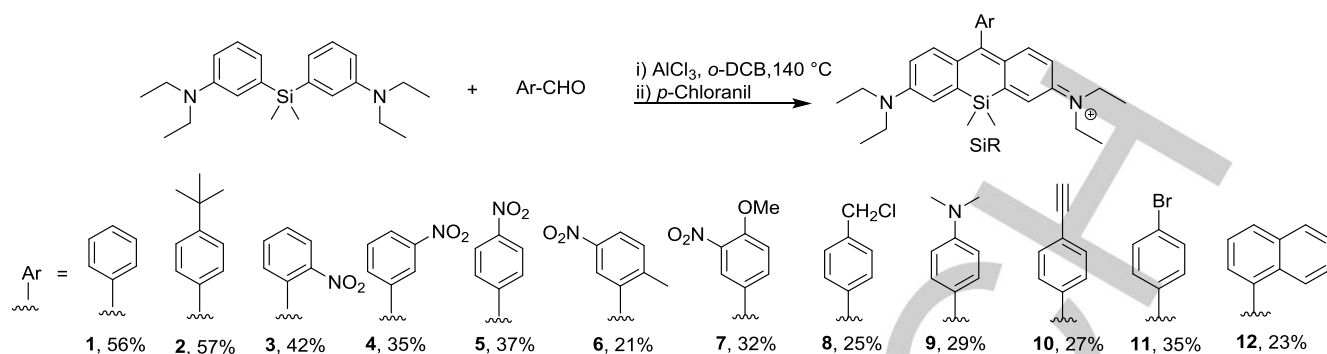
Fluorescent probes are the powerful and most convenient chemical tools to investigate biological processes.^[1] In particular, red and near-infrared (NIR) fluorophores with excitation and emission in the spectral region of 600-900 nm are of high interest. Unlike visible-light fluorophores, red and near-infrared (NIR) fluorophores exhibit low autofluorescence interference, deep tissue penetration, and minimal photodamage to biological samples.^[2] Therefore, various fluorescent probes for detecting

specific targets have been developed based on red to NIR emitters.^[3] Among the fluorophores, rhodamine is often used since it exhibits high photostability, good water solubility, and strong fluorescence quantum yield. However, rhodamine-based fluorophores usually show absorption and emission wavelengths below 600 nm, which limits their application for bioimaging in living systems.^[4]

Replacement of the bridging oxygen by silicon has been shown to dramatically red-shift their absorption wavelengths to the range of 630-660 nm, matching the commercial red laser very well.^[5] Notably, silicon-substituent improves their resistance to photobleaching, while retaining the key advantages that rhodamines have many biological applications, such as water-solubility, pH independency of photophysical properties, and mitochondrial localization in cells.^[6] The bathochromic shift results from the relatively low-lying LUMO energy levels, due to $\sigma^*-\pi^*$ conjugation resulting from interaction of the σ^* orbital of silicon atom with the π^* system of the xanthene moiety.^[6b]

The first silicon-substituted xanthene fluorophore, TMDHS(2,7-bis(dimethylamino)-9,9-dimethyl-9-sila9H-anthracenium), was reported by Xiao et al in 2008.^[7] Subsequently, Nagano and co-workers developed a series of silicon-substituted rhodamines (SiRs) with functional group at *meso*-position via nucleophilic addition of aryl lithium reagents to the Si-xanthone.^[8] In 2017, Lavis and Sparr et al. developed a new way of synthesis of SiR through reaction of the intermediate bisnucleophiles reacted with anhydride or carboxylic acid esters electrophiles.^[9] Aryllithium or aryl Grignards are used in both synthetic methods, which are incompatible with many functional groups, thus require the use of complex protection strategies. Urano and Kramer et al. synthesized the SiR by coupling the triflate of xanthone with boroxines,^[10] this method usually need multi-step synthesis. Therefore, new strategies are urgent for construction of SiR containing functional groups for bioimaging application.

FULL PAPER



Scheme 1. Synthetic procedures and chemical structure of SiRs 1-12.

In other hand, mitochondria are essential organelles and play roles in many important metabolic processes such as signaling, cellular differentiation and apoptosis, and storage of calcium ions.^[11] Mitochondria act as the power generators of the cell and their temperature variation may be a sign of the status of mitochondrial energetics.^[12] In some diseases, cellular dysfunctions, originating in disordered energy metabolism, might be revealed by abnormal changes of local temperature in mitochondria.^[13] However, monitoring in real-time the local temperature within mitochondria is extremely challenging.^[14] Several exciting research on molecular thermometers targeting mitochondria have been reported,^[15] however, challenges remain in the NIR dyes with high photostability, in which contain a fixable unit to form stable covalent bonds with biomacromolecules.

We noticed that Wang et al. reported a simple synthesis for the Si-rhodamines (SiRs) using *p*-toluenesulfonic acid monohydrate catalyst without any solvent in sealed tube.^[16] The authors warn us of potential dangers (an explosion occurred when we repeated the experiment) and the solid-state reaction is heterogeneous reaction. Furthermore, SiRs synthesized by this method contain both *p*-toluenesulfonate anion and Cl anion, leading to very difficult purification. Herein, we reported a general approach via a condensation reaction of diarylsilylene ether and arylaldehyde in *o*-dichlorobenzene (*o*-DCB) to construct a series of Si-rhodamine bearing various functional substituents, such as $-\text{NO}_2$, $-\text{CH}_2\text{Cl}$, $-\text{N}(\text{CH}_3)_2$ and $-\text{C}\equiv\text{CH}$ with moderate to high yield. We then investigated their spectroscopic properties in which the fluorescence properties are well controlled by the photoinduced electron transfer (PET) mechanism, temperature-dependent emissive behaviour and photostability. SiR **8**, containing chloromethyl unit, which can covalently immobilizes the dyes onto the mitochondrial via “click-type” reaction between the benzyl chloride and protein sulfhydryls, exhibits excellent properties for visualizing the morphology and monitoring the temperature change of mitochondrial with high photostability.^[17] Our work provides a promising strategy to design functional fluorophores and a new platform for real time and local temperature monitoring in mitochondria.

Results and Discussion

Optimization of reaction conditions and synthesis. Initially, the effects of solvents and catalysts in the condensation reactions were examined. The results are shown in Table S1. Among

the solvents examined, the use of high boiling solvents is essential for this reaction, and *o*-dichlorobenzene was found to be optimal solvent. Among the several acid catalysts screened, AlCl_3 was recognized as being the most effective, which afforded the SiR **1** product in 56% isolated yield. On the basis of these results, we examined the applicability and scope to other aryl aldehydes. A variety of SiRs in some cases containing various functional substituents were then synthesized in a one step process. Accordingly, the present reaction provides a simple and general procedure for the preparation of SiRs.

Spectroscopic Properties. Usually, rhodamine-based fluorophores show absorption and emission wavelength around 530 and 550 nm, respectively. SiRs **1-12** display a narrow absorption band in the range of 650-666 nm with high molar extinction coefficients (usually above 10^5 M/cm) and a weak shoulder around 610 nm (Figure 1a, and Table S3). Replacement of oxygen by silicon results in a red shift of ca. 120 nm for the main absorption and emission band relative to the analogous band of Rho 6G. The main absorption band can be assigned as the main electronic band of the $S_0 \rightarrow S_1$ transition. Depending on the substituent in the meso position, the absorption maximum appears between 666 nm for SiR **5** with the strongest electron acceptor and 652 nm for SiR **9** with the strongest electron donor (Table 1). An increase of the substituent's electron accepting nature results in a bathochromic shift of the absorption and emission bands. The absorption energy follows a linear dependence with the electron donor strength of R according to the Hammett constant σ_p (Figure 1b). Although the X-ray structure of SiR **5** reveals that the meso-aryl group and the fluorophore are almost orthogonal for approximately 87° in crystals (Figure S1), certain degree of conjugation and a certain influence of the electronic nature of R on the spectroscopic properties can be expected.^[18]

The emission bands of SiRs **1-12** mirror images of their $S_0 \rightarrow S_1$ transition bands with moderate Stokes shifts are observed. The absorption and emission maxima are almost independent of the solvent polarity with a maximum solvent shift of 7 nm in CH_2Cl_2 and CH_3CN . These features suggest that the emission originates from the weakly polar and non-relaxed S_1 state of the chromophores. The full width at half-maximum height of the absorption and emission spectra of SiRs **1-12** are narrow at approximately below 40 nm, similar to typical BODIPY derivatives, which has the advantages of high throughput efficiency, sensor's sensitivity and resolution (Table 1).

FULL PAPER

Table 1. Photophysical properties of SiRs 1-12 measured in CH₂Cl₂ and CH₃CN.

	Solvent	λ_{abs} [nm]	Fwhm _{abs} [nm]	λ_{em} [nm]	Fwhm _{em} [nm]	$\Delta V_{\text{abs-em}}^{[a]}$ [cm ⁻¹]	$\Phi_F^{[b]}$	$\tau_f^{[c]}$ [ns]	$k_r^{[d]}$ [10 ⁸ s ⁻¹]	$k_{nr}^{[e]}$ [10 ⁸ s ⁻¹]	ϵ M ⁻¹ cm ⁻¹
1	CH ₂ Cl ₂	655	29	669	37	319	0.35	3.09	1.13	2.10	132800
	CH ₃ CN	652	33	671	38	434	0.35	2.50	1.40	2.60	117200
2	CH ₂ Cl ₂	653	42	666	38	299	0.34	2.68	1.27	2.46	97600
	CH ₃ CN	650	42	667	39	392	0.31	1.77	1.75	3.90	97100
3	CH ₂ Cl ₂	666	38	677	44	244	0.40	4.07	0.98	1.47	97800
	CH ₃ CN	661	42	680	43	423	0.12	1.45	0.83	6.07	96800
4	CH ₂ Cl ₂	665	31	677	38	267	0.32	3.06	1.05	2.22	109100
	CH ₃ CN	660	36	676	39	359	0.23	2.31	1.00	3.33	92900
5	CH ₂ Cl ₂	666	29	679	37	287	0.17	1.57	1.08	5.29	98400
	CH ₃ CN	661	33	677	38	358	0.10	1.04	0.96	8.65	88000
6	CH ₂ Cl ₂	666	30	678	37	266	0.55	5.31	1.04	0.85	109600
	CH ₃ CN	661	35	677	39	358	0.34	4.64	0.73	1.42	99100
7	CH ₂ Cl ₂	664	30	675	36	245	0.33	3.33	0.99	2.01	111700
	CH ₃ CN	659	34	674	38	338	0.18	2.78	0.65	2.95	96400
8	CH ₂ Cl ₂	658	29	674	35	361	0.40	2.40	1.67	2.50	113000
	CH ₃ CN	655	33	672	37	382	0.26	1.95	1.33	3.80	128000
9	CH ₂ Cl ₂	652	39	667	36	345	<0.01	--	--	--	178500
	CH ₃ CN	650	44	666	39	370	<0.01	--	--	--	183000
10	CH ₂ Cl ₂	663	28	676	35	290	0.27	2.45	1.10	2.98	125000
	CH ₃ CN	656	32	673	37	385	0.25	1.91	1.31	3.93	144100
11	CH ₂ Cl ₂	659	32	673	38	316	0.41	3.11	1.32	1.90	158300
	CH ₃ CN	655	36	672	38	386	0.34	2.26	1.50	2.92	191000
12	CH ₂ Cl ₂	663	31	677	38	312	0.80	5.30	1.51	0.38	145200
	CH ₃ CN	660	32	674	37	315	0.65	4.54	1.43	0.77	190000

[a] Stokes shift. [b] Fluorescence quantum yield using Zinc phthalocyanine ($\Phi_F = 0.30$ in 1% pyridine in toluene) as the standard. The standard errors are less than 5%. [c] fluorescence lifetime. [d] Radiation rate constant. [e] Non-radiation rate constant.

Photostability is an important parameter especially in application of biological imaging for long-term observation. SiRs display high stability and can persist continuous exposure to irradiation for 40 min using a laser beam (635 nm, 200 mW/cm²). Whereas, methylene blue (MB), with a similar absorption band with SiR, shows significant photobleaching after irradiation (Figure 1c).

We envision that the rotation of the diethylamino and *meso*-phenyl group can lead to the decreasing of fluorescent intensity with the increasing temperature.^[19] Therefore, we explored the temperature sensitivity of SiR **8** in sodium phosphate buffer solution. As shown in Figure 1d-e, the fluorescence intensity decreases gradually as the temperature increases from 10 to 45 °C, and SiR **8** maintains its performance after going through several temperature cycle. Accordingly, the fluorescence lifetime reduces from 1.66 ns at 10 °C, 1.37 ns at 20 °C to 0.74 ns at 45 °C. Moreover, fluorescence intensity is not greatly affected by pH (Figure S2). These results show that SiR **8** could be used as a molecular thermometer by correlating its fluorescence intensity with temperature.

All the SiRs have moderate to high fluorescence quantum yields (0.30-0.80), except SiR **9**, which fluorescence is quenched due to the PET from N(CH₃)₂ to the fluorophore. As expected, protonation at the aniline-N atom suppresses the quenching process and leads to a revival of fluorescence. Figure S3 demonstrates the potential of SiR **9** as a pH light-up probe, analysis of titration curves yields a pKs of 3.4. SiR **12** displays relatively high

fluorescence quantum yield up to 0.80 in dichloromethane due to the restriction of free rotation of *meso*-substituent resulting from the large steric hindrance of naphthyl group. The fluorescence decay profiles could be described with a single-exponential fit with fluorescence life times in the 1.04–5.31 ns range (Table 1).

DFT calculations. DFT and TD-DFT calculations were carried out to understand the spectroscopic behaviours. The substitution of oxygen by silicon destabilize HOMO and stabilize LUMO energy, thus a smaller energy gap is obtained and large red shift is achieved. The low-lying LUMO energy level can be attributed to the $\sigma^*-\pi^*$ interaction between the σ^* orbital of silicon atom with the π^* system of the xanthene moiety. The HOMO energy increase is caused by the inductive electron-donating effect of the dimethylsilyl group relative to oxygen.^[7] (Figure S3). Usually, quenching of the original fluorescent emission will take place when the PET process is followed by a non-luminescent adiabatic process returning to the ground state. The PET process may be rationalized pictorially in terms of simple molecular orbital theory, which was first developed by Weller^[20] and has become a prevalent tool to discuss the fluorescence on-off.^[10a, 21] The *meso*-aryl group and the fluorophore is almost orthogonal, the emitting properties are well explained by PET mechanism. TD-DFT calculations display that the main component of the allowed S₀→S₁ transition of SiRs **1-8** and **10-12** and protonated **9** is the fluorophore localized HOMO→LUMO (Table S3). Scheme 2 shows the possible pathways of fluorescence emission and

FULL PAPER

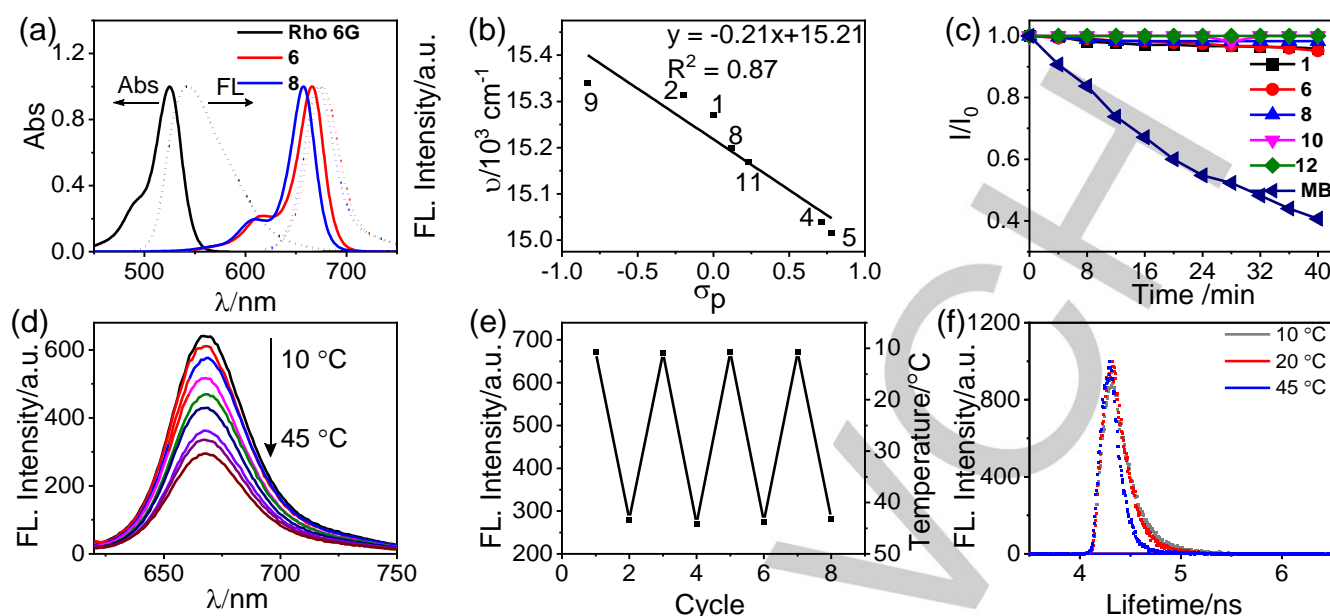
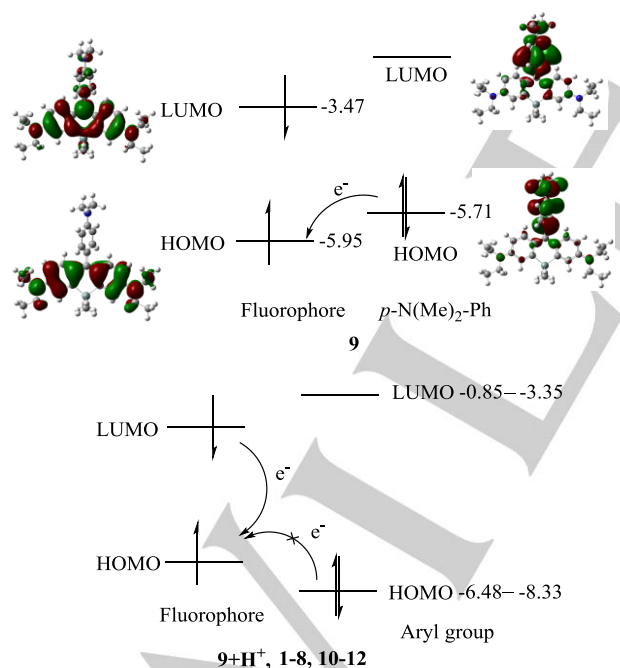


Figure 1. (a) Absorption (solid line) and fluorescence (dot line) spectra of Rho 6G, SiR **6** and **8** in dichloromethane. (b) Absorption maxima in wavenumbers versus Hammett constant. (c) Comparison of photostability of methylene blue (MB), SiR **1**, **6**, **8**, **10** and **12** in DCM at 4 min intervals determined using a laser beam (635 nm, 200 mW/cm²) over an irradiation period of 40 min ($c=10^{-5}$ M). (d) Fluorescence spectra of SiR **8** (1 μM in 0.1 M sodium phosphate buffer, pH 7.4 containing 1% DMSO) recorded at different temperature values. (e) Cycle of temperature change and intensity at 666 nm. All data were obtained using an excitation wavelength of 610 nm. (f) Time-resolved FL decay curves of SiR **8** measured at 10, 20 and 45.



Scheme 2. HOMO and LUMO energy level of the fluorophore and the aryl moiety. These values were obtained in CH_2Cl_2 calculated with the polarisable continuum model (PCM) by using the B3LYP functional with 6-31+G(d) basis sets.

electron transfer processes. We first look into the electron distribution and pick out the orbitals mainly localized on fluorophore part to form the left column; similarly, the right column comes from orbitals mainly distributed on the *meso*-aryl part. In

case of SiR **9**, the electron transfer from aniline group to fluorophore is possible due to the fact that the HOMO of the substituent is located above the HOMO of the fluorophore. Electron transfer takes place during the electrons reorganization to its lowest vibrational state on the S_1 energy surface, which prohibits the electron on the LUMO of fluorophore from going back directly, which could explain the low fluorescence quantum yield of SiR **9** (Scheme 2). The lowest transition state of SiR **9** is predicted by TD-DFT using B3LYP functional to be associated with HOMO localized on aniline group to LUMO localized on fluorophore with small oscillator strengths, the calculated oscillator strengths of the corresponding emission ($S_1 \rightarrow S_0$) is zero, therefore, S_1 is dark state (Table S4). However, the energy levels of the molecular orbitals change greatly when protonated, which lead to significant changes in energy sequences of these frontier orbitals, the LUMO orbital of the receptor is higher than the LUMO of the fluorophore and the HOMO orbital of the receptor is lower than the HOMO of the fluorophore, thus electron transfer from *meso*-N,N-dimethylaniline group to fluorophore is forbidden (Scheme 2). The calculated emission have large oscillator strengths thus $S_1 \rightarrow S_0$ is radiative process. This explains the fluorescence enhancement phenomena after the addition of the acid. Similar cases are shown in Scheme 2 for SiRs **1-8** and **10-12**. DFT calculations using CAM-B3LYP/6-31+G(d) display the same trend with the B3LYP functional (Figure S5).

Evaluation of the mitochondria-targeting capability. Cell viability was investigated first before applying SiR **8** in cellular imaging. Apparently, more than 85% of the HepG2 cells were survived under the dosage of 40 $\mu\text{g}/\text{mL}$ SiR **8** (Figure S6), indicating the good biocompatibility. We then evaluated the imaging

FULL PAPER

ability of SiR **8** in live cells by confocal laser scanning microscopy (CLSM). Filamentous structures of the mitochondria morphology were observed in the CLSM images (Figure S7). The fluorescence intensity of SiR **8** in the live cells obviously relied on the

concentration of SiR **8** and incubation time. To avoid any unnecessary leakage, 10 $\mu\text{g/mL}$ SiR **8** and 30 min incubation time were selected for the next experimental conditions.

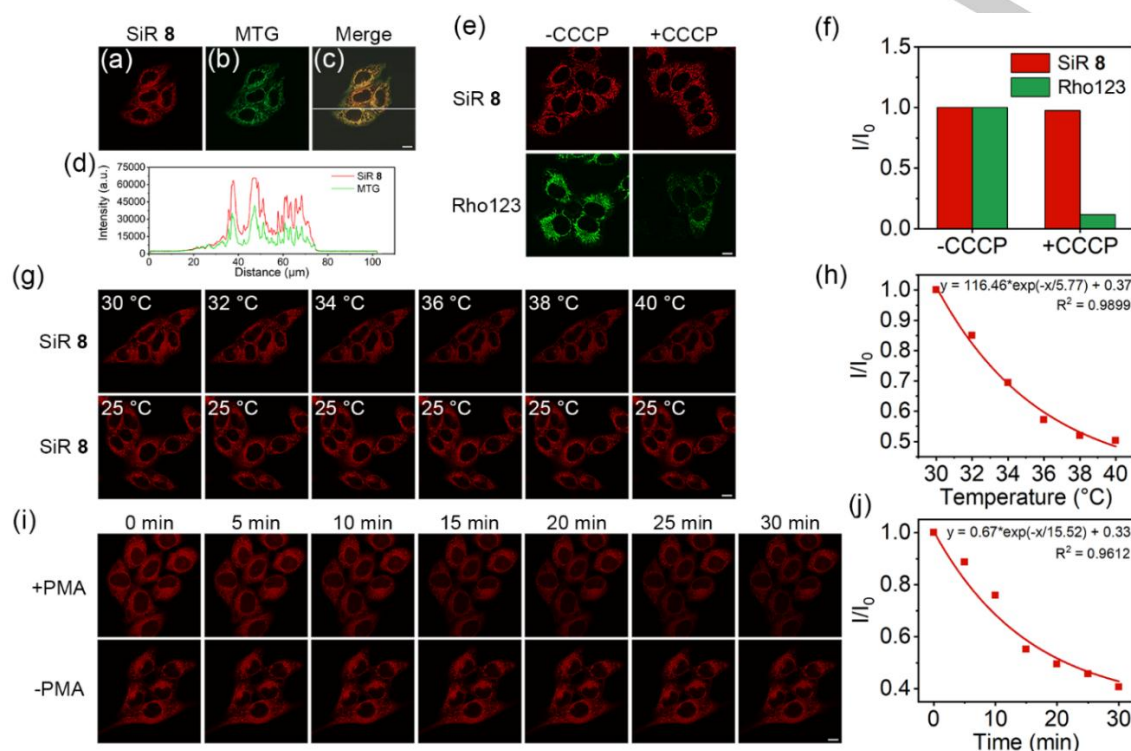


Figure 2. Confocal fluorescence imaging for living cells. (a) CLSM of SiR **8** (10 $\mu\text{g/mL}$) in live HepG2 cells. (b) CLSM of Mito Tracker Green (MTG, 100 nM) in live HepG2 cells. (c) Merged image of (a), (b) and bright field image. (d) Fluorescence intensity profile of the marked line in (c). (e) Fluorescence images of HepG2 cells stained with SiR **8** (10 $\mu\text{g/mL}$) and Rho123 (50 nM), and then treated with (right side) and without (left side) CCCP (10 μM). (f) Normalized fluorescence intensity plots of HepG2 cells corresponding to (e). (g) Fluorescence images of SiR **8** (10 $\mu\text{g/mL}$) in HepG2 cells exposed to external media fixed at 30, 32, 34, 36, 38 and 40 degree centigrade, respectively (top). Fluorescence images of SiR **8** (10 $\mu\text{g/mL}$) in HepG2 cells exposed to external media at room temperature (bottom). (h) Changes in the fluorescence intensity of SiR **8** in HepG2 cells exposed to external media of different temperature corresponding to (g). (i) Real-time monitoring of mitochondrial-temperature changes in PMA-stimulated HepG2 cells ($t = 0, 5, 10, 15, 20, 25$ and 30 min). (j) Changes in the fluorescence intensity of SiR **8** (10 $\mu\text{g/mL}$) with stimulation time corresponding to (i). Scale bars: 10 μm .

We then studied the cellular uptake mechanism of SiR **8**. The HepG2 cells were cultured with SiR **8** at 4 $^{\circ}\text{C}$ and 37 $^{\circ}\text{C}$ for 30 min, respectively. No significant divergence in fluorescence intensity was shown in Figure S8, indicating that the cellular uptake of SiR **8** may be non-energy-dependent mechanism, like physical adhesion and penetration. Additionally, because the clathrin- and caveolae-mediated endocytosis processes are the most extensively studied endocytosis pathways for eukaryotic cells, the effects of chemical inhibitors on the cellular internalization of SiR **8** were explored. HepG2 cells were incubated with dynasore (an inhibitor of clathrin-mediated endocytosis) and genistein (an inhibitor of caveolae-mediated endocytosis) to study the roles of the endocytosis process of SiR **8**. No obvious difference of the fluorescence intensity was observed in live cells with drug treatment compared with the control group (Figure S9). The above results demonstrated that the physical adhesion and then penetration was the main pathway for SiR **8** endocytosis process.

To access the mitochondria-targeting ability of SiR **8**, HepG2 cells were costained with SiR **8** and commercial fluorescent trackers (Mito Tracker Green, Lyso Tracker Green and Hoechst 33342, respectively). The fluorescence from SiR **8** almost completely overlapped with that from Mito Tracker Green (Figure 2a-c). An intensity profile of the mitochondria marked with a line in Figure

2c was used to investigate the degree of the colocation as demonstrated in Figure 2d. The well-matched intensity peaks confirm the excellent mitochondria-targeting ability of SiR **8** in live cells.^[22] In addition, CLSM images of live HepG2 cells stained with 10 $\mu\text{g/mL}$ SiR **8** at different sections through the zaxis were performed in ESI, Figure S10. On the contrary, the fluorescence from SiR **8** didn't overlap with that from Lyso Tracker Green (Figure S11) and Hoechst 33342 (Figure S12). These results demonstrated that the high selectivity of SiR **8** to mitochondria. By the way, the generic mitochondrial targeting feasibility of SiR **8** was tested on other cell lines including carcinoma cell line (human mammary cancer MCF-7 cells) and normal cell lines (human normal liver L-02 cells and mouse embryonic fibroblast 3T3-L1 cells). The whole cell lines displayed clear filamentous structures (Figure S13), illustrating great mitochondria targeting efficiency of SiR **8** in different cell lines.

To test the immobilizing ability of SiR **8** in mitochondria, carbonyl cyanide 3-chlorophenylhydrazone (CCCP), a type of protonophore that can decrease the mitochondrial membrane potential (MMP),^[23] was utilized to conduct a mitochondrial uncoupling experiment. HepG2 cells were cultured with SiR **8** and Rhodamine 123 at 37 $^{\circ}\text{C}$ for 30 min, respectively. Rho123 is an electrostatic-attraction based cationic mitochondrial probe which can

FULL PAPER

disengagement from mitochondria when MMP is abolished. Then the above cells were all incubated with 10 μ M CCCP for another 1 h. The SiR **8**-stained mitochondria performed excellent fluorescence stability after CCCP incubation while the Rho123-stained showed significant fluorescence intensity decrease (Figure 2e and 2f). Moreover, the fluorescence intensity of Rho123 (green channel) displayed much weaker in the presence of SiR **8** (Figure S14), which may due to the competitive reaction of SiR **8** with nucleophiles in mitochondria. The results demonstrated that SiR **8** exhibited stronger binding capability. Notably, the fluorescence intensity of SiR **8**-stained HepG2 cells changed negligibly while that of Rho123 decreased obviously within 12 min (Figure S15), illustrating the high photostability of SiR **8**. Compared to commercial probe Rho123, our new probe SiR **8** exhibits brilliant imaging capability with MMP decreased, and shows stronger binding capacity to mitochondria and excellent stability, which could be attributed to the covalent bonding between chloromethyl group of SiR **8** and nucleophiles in mitochondria.

Mitochondrial temperature quantification through CLSM imaging of living cells. SiR **8** was also utilized to monitor the local temperature in the mitochondria of living cells by CLSM. HepG2 cells stained with SiR **8** were incubated with culture media at different temperatures. The fluorescence intensity of SiR **8** gradually decreased as the culture temperature rose from 30 to 40 $^{\circ}$ C (Figure 2g). While the fluorescence intensity of SiR **8** at room temperature for the same duration of time didn't change (Figure 2g). The results demonstrated that SiR **8** could be used as an indicator for probing mitochondrial temperature. It was worth noting that changes in fluorescence intensity was not linearly related to the alteration of living cells medium temperature (Figure 2h), which could be attributed that living cells may have self-regulating ability to against the changes in the external temperature. Moreover, phorbol 12-myristate-13-acetate (PMA) as a chemical reagent to activate the protein kinase C system was utilized to stimulate HepG2 cells, which could cause remarkable change in mitochondrial temperature.^[24] As displayed in Figure 2i and Figure 2j, during the 30 min stimulation process, the fluorescence intensity of SiR **8** apparently decreased, which indicated the increasing mitochondrial temperature of HepG2 cells. Nevertheless, the fluorescence intensity of no PMA-treated HepG2 cells changed slightly. All the above results confirmed that SiR **8** could have the excellent ability to monitor the mitochondrial temperature in living cells.

Conclusion

We have developed a general approach to prepare SiR bearing various functional groups without protection with moderate yields. These SiRs display moderate to high fluorescence quantum efficiency, high photostability and NIR emitting, and their NIR fluorescence properties could be controlled through the PET mechanism. DFT and TD-DFT calculations rationalize the OFF-ON sensing and PET mechanism. A fixable molecular thermometer, to trace local mitochondrial temperature has been established because positively charged probe SiR **8** has a chloromethyl group as an anchoring unit, which enables its permanent immobilization into mitochondria, so that it maintains sensitivity toward temperature. Therefore, we envisage that the fixable thermometer SiR **8** will help improve diagnostics and test dynamic monitoring of mitochondrial temperature as a means of distinguishing

between physiological and pathological conditions or screening for potential new mitochondrial targeting drugs.

Experimental Section

Materials and Instruments. All the starting materials were obtained from commercial suppliers and used as received. Details are in Supporting Information.

General synthetical method. Diarylsilylether (100 mg, 0.3 mmol), arylaldehyde (1.5 mmol) and AlCl_3 (0.3 mmol) were added in a 10 mL Schlenk, then added 2 mL o-dichlorobenzene and heated to 140 $^{\circ}$ C for 8 hours. After cooling to room temperature, the reaction mixture was dissolved in dichloromethane/methanol (2 mL/2 mL), to which p-chloranil (110 mg, 0.45 mmol) was added. The reaction mixture was stirred at room temperature 12 h, then filtrated and evaporated under reduced pressure. The residue solid was purified by column chromatography on silica gel (dichloromethane: methanol = 20: 1) to afford compound SiR as a dark blue solid.

Spectroscopic measurements. Fluorescence spectra and the fluorescence lifetimes of the samples were determined with a Horiba Jobin Yvon Fluorolog-3 spectrofluorimeter. The goodness of the fit of the single exponential decays were judged using the chisquared (χ_{R2}) and the autocorrelation function $C(j)$ values. Low residuals ($\chi_{R2} < 1.2$) were consistently observed. For samples in solution, absorption and emission measurements were carried out in 1x1 cm quartz cuvettes. The luminescence quantum yields were measured using Zinc phthalocyanine ($\Phi_F = 0.30$ in 1% pyridine in toluene) as a reference.^[25] The quantum yield Φ_F as a function solvent polarity is calculated using the following equation.

$$\Phi_{\text{sample}} = \Phi_{\text{std}} \left[\frac{I_{\text{sample}}}{I_{\text{std}}} \right] \left[\frac{A_{\text{std}}}{A_{\text{sample}}} \right] \left[\frac{n_{\text{std}}^2}{n_{\text{sample}}^2} \right] \quad (1)$$

Where subscript sample and std denote the sample and standard, respectively, Φ is quantum yield, I is the integrated emission intensity, A stands for the absorbance, n is refractive index.

The rate constants of radiative (k_r) and nonradiative (k_{nr}) deactivation were calculated from the measured fluorescence quantum yield and fluorescence lifetime (τ) according to equations (2) and (3):

$$k_r = \Phi/\tau \quad (2)$$

$$k_{nr} = (1-\Phi)/\tau \quad (3)$$

Computational details. The ground state structures were optimized using density functional theory (DFT) with B3LYP and CAM-B3LYP functional and 6-31+G(d) basis set. The excited state related calculations were carried out with the time dependent DFT (TD-DFT), based on the optimized structure of the ground state. The polarizable continuum model (PCM) is used in CH_2Cl_2 to model solvation effects. All these calculations were performed with Gaussian 09.^[26]

Crystallographic data. The X-ray crystallographic coordinates for the structures reported in this article have been deposited at the Cambridge Crystallographic Data Centre (CCDC) under deposition numbers CCDC 1985857. These data can be obtained free of charge from The Cambridge Crystallographic Data Centre via www.ccdc.cam.ac.uk/data_request/cif.

Co-localization assay. The HepG2 cells were washed with PBS and further stained with 10 μ g/mL SiR **8**. After incubated for 30 min, the cells were washed with PBS twice to remove the unbound molecules. Subsequently, the cells were stained with 100 nM MitoTracker Green (MTG). MitoTracker Green were excited at 488 nm with an argon ion laser, and the emission was collected from 500 to 550 nm. All images were

FULL PAPER

analyzed by a ZEN imaging software. To evaluate whether the as-synthesized SiR 8 can specifically target the mitochondria even if the mitochondrial membrane potential (MMP) changed or vanished, 10 $\mu\text{g}/\text{mL}$ as-treated SiR 8 was firstly added into the HepG2 cells for 30 min at 37 °C. 50 nM Rho123 solution was injected into the other cell dish. After incubated for 30 min, the cells were washed with PBS twice to remove the unbound molecules. Afterwards, the media were replaced with fresh DMEM containing CCCP (10 μM) and the cells were incubated for another 1 h, respectively; finally, the cells were washed and cell imaging was performed as mentioned above.

In situ quantification of mitochondrial temperature. The stained HepG2 cells were heated to the set temperature (30, 32, 34, 36, 38 and 40 °C). When the set temperature was reached, turn on the laser light source for snapping. In addition, at room temperature, take confocal images for the same duration of time as control. The other way to change mitochondrial temperature is to use chemicals. The stained cells was treated with 1 mL DMEM culture contained 80 μM PMA. Before imaging, the redundant reagents were removed by washing with PBS three times. All images were analyzed by ImageJ software.

Acknowledgements

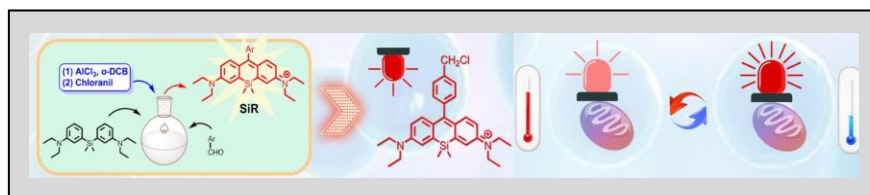
We thank the National Natural Science Foundation of China (No. 21871072 and 21775166) for financial support, the Program for High-Level Innovation Team in Universities of Zhejiang Province, the Natural Science Foundation for Distinguished Young Scholars of Jiangsu Province (BK20180026).

Keywords: Si-rhodamine • Dyes and Pigments • NIR emission • PET • Cell imaging

- [1] a) *Nat. Cell. Biol.* **2009**, *11*, 1165-1165; b) J. Zhang, R. E. Campbell, A. Y. Ting and R. Y. Tsien, *Nat. Rev. Mol. Cell. Biol.* **2002**, *3*, 906-918.
- [2] a) H. Lu, J. Mack, Y. Yang and Z. Shen, *Chem. Soc. Rev.* **2014**, *43*, 4778-4823; b) H. Lu, S. Shimizu, J. Mack, Z. Shen and N. Kobayashi, *Chem. Asian.* **2011**, *6*, 1026-1037; c) Y. Sun, H. Yuan, L. Di, Z. Zhou, L. Gai, X. Xiao, W. He and H. Lu, *Org. Chem. Front.* **2019**, *6*, 3961-3968.
- [3] a) L. Yuan, W. Lin, K. Zheng, L. He and W. Huang, *Chem. Soc. Rev.* **2013**, *42*, 622-661; b) M. Kaur and D. H. Choi, *Chem. Soc. Rev.* **2015**, *44*, 58-77; c) Z. Guo, Y. Ma, Y. Liu, C. Yan, P. Shi, H. Tian and W.-H. Zhu, *Sci. China Chem.* **2018**, *61*, 1293-1300; d) J. Chin and H.-J. Kim, *Coord. Chem. Rev.* **2018**, *354*, 169-181; e) V. J. Pansare, S. Hejazi, W. J. Faenza and R. K. Prud'homme, *Chem. Mater.* **2012**, *24*, 812-827.
- [4] a) L. M. Wysocki, J. B. Grimm, A. N. Tkachuk, T. A. Brown, E. Betzig and L. D. Lavis, *Angew. Chem. Int. Ed.* **2011**, *50*, 11206-11209; b) L. M. Wysocki and L. D. Lavis, *Curr. Opin. Chem. Biol.* **2011**, *15*, 752-759; c) M. Beija, C. A. Afonso and J. M. Martinho, *Chem. Soc. Rev.* **2009**, *38*, 2410-2433.
- [5] Y. Q. Sun, J. Liu, X. Lv, Y. Liu, Y. Zhao and W. Guo, *Angew. Chem. Int. Ed.* **2012**, *51*, 7634-7636.
- [6] a) L. Wang, W. Du, Z. Hu, K. Uvdal, L. Li and W. Huang, *Angew. Chem. Int. Ed.* **2019**, *58*, 14026-14043; b) T. Ikeno, T. Nagano and K. Hanaoka, *Chem. Asian. J.* **2017**, *12*, 1435-1446; c) T. Wang, Q.-J. Zhao, H.-G. Hu, S.-C. Yu, X. Liu, L. Liu and Q.-Y. Wu, *Chem. Commun.* **2012**, *48*, 8781-8783; d) Y. Kushida, T. Nagano and K. Hanaoka, *Analyst.* **2015**, *140*, 685-695; e) O. Murata, Y. Shindo, Y. Ikeda, N. Iwasawa, D. Citterio, K. Oka and Y. Hiruta, *Anal. Chem.*, **2020**, *92*, 966-974; f) E. Kozma, G. Estrada Girona, G. Paci, E. A. Lemke and P. Kele, *Chem. Commun.*, **2017**, *53*, 6696-6699.
- [7] M. Fu, Y. Xiao, X. Qian, D. Zhao and Y. Xu, *Chem. Commun.* **2008**, *15*, 1780-1782.
- [8] a) T. Egawa, Y. Koide, K. Hanaoka, T. Komatsu, T. Terai and T. Nagano, *Chem. Commun.* **2011**, *47*, 4162-4164; b) Y. Koide, Y. Urano, K. Hanaoka, W. Piao, M. Kusakabe, N. Saito, T. Terai, T. Okabe and T. Nagano, *J. Am. Chem. Soc.* **2012**, *134*, 5029-5031; c) Y. Koide, Y. Urano, K. Hanaoka, T. Terai and T. Nagano, *ACS Chem. Biol.* **2011**, *6*, 600-608.
- [9] a) J. B. Grimm, T. A. Brown, A. N. Tkachuk and L. D. Lavis, *ACS Central Sci.* **2017**, *3*, 975-985; b) C. Fischer and C. Sparr, *Angew. Chem. Int. Ed.* **2018**, *57*, 2436-2440.
- [10] a) K. Umezawa, M. Yoshida, M. Kamiya, T. Yamasoba and Y. Urano, *Nat. Chem.* **2017**, *9*, 279-286; b) T. Kanagasundaram, A. Timmermann, C. S. Kramer and K. Kopka, *Beilstein J. Org. Chem.* **2019**, *15*, 2569-2576.
- [11] H. M. McBride, M. Neuspiel and S. Wasiak, *Curr. Biol.* **2006**, *16*, 551-560.
- [12] A. I. Jonckheere, J. A. Smeitink and R. J. Rodenburg, *J. Inherited Metab. Dis.* **2012**, *35*, 211-225.
- [13] X. Emily Guo, B. Ngo, A. Sandaldjian Modrek and W.-H. Lee, *Curr. Drug. Targets.* **2014**, *15*, 2-16.
- [14] a) X. Zhang, Q. Sun, Z. Huang, L. Huang and Y. Xiao, *Mater. Chem. B.* **2019**, *7*, 2749-2758; b) M. M. Ogle, A. D. Smith McWilliams, M. J. Ware, S. A. Curley, S. J. Corr and A. A. Martí, *J. Phys. Chem. B.* **2019**, *123*, 7282-7289.
- [15] a) M. Homma, Y. Takei, A. Murata, T. Inoue and S. Takeoka, *Chem. Commun.* **2015**, *51*, 6194-6197; b) H. Huang, H. Li, J.-J. Feng and A.-J. Wang, *Microchim. Acta.* **2017**, *184*, 1215-1221; c) Z. Huang, N. Li, X. Zhang, C. Wang and Y. Xiao, *Anal. Chem.* **2018**, *90*, 13953-13959; d) J. Qiao, C. Chen, D. Shangguan, X. Mu, S. Wang, L. Jiang and L. Qi, *Anal. Chem.* **2018**, *90*, 12553-12558; e) M. H. Lee, J. H. Han, J.-H. Lee, H. G. Choi, C. Kang and J. S. Kim, *J. Am. Chem. Soc.* **2012**, *134*, 17314-17319; f) S. Arai, S. C. Lee, D. Zhai, M. Suzuki, Y. T. Chang, *Sci. Rep.*, **2015**, *4*, 6701.
- [16] B. Wang, X. Chai, W. Zhu, T. Wang and Q. Wu, *Chem. Commun.* **2014**, *50*, 14374-14377.
- [17] M. Poot, Y. Z. Zhang, J. A. Krämer, K. S. Wells, L. J. Jones, D. K. Hanzel, A. G. Lugade, V. L. Singer and R. P. Haugland, *J. Histochem. Cytochem.*, **1996**, *44*, 1363-1372.
- [18] C. Hansch, A. Leo and R. Taft, *Chem. Rev.* **1991**, *91*, 165-195.
- [19] a) T. Bai and N. Gu, *Small*, **2016**, *12*, 4590-4610; b) L. Chen and A. Wood, *Bioelectromagnetics*, **2009**, *30*, 583-590.
- [20] A. Weller, *Pure. Appl. Chem.* **1968**, *16*, 115-124.
- [21] a) H. Lu, S. Zhang, H. Liu, Y. Wang, Z. Shen, C. Liu and X. You, *J. Phys. Chem. A.* **2009**, *113*, 14081-14086; b) H. Guo, Y. Jing, X. Yuan, S. Ji, J. Zhao, X. Li and Y. Kan, *Org. Biomol. Chem.* **2011**, *9*, 3844-3853; c) H. Sunahara, Y. Urano, H. Kojima and T. Nagano, *J. Am. Chem. Soc.* **2007**, *129*, 5597-5604.
- [22] S. Hong, X. Zhang, R. J. Lake, G. T. Pawel, Z. Guo, R. Pei and Y. Lu, *Chem. Sci.* **2020**, *11*, 713-720.
- [23] M. L. Lim, T. Minamikawa and P. Nagley, *FEBS Lett.* **2001**, *503*, 69-74.
- [24] C. D. Kang, B. K. Lee, K. W. Kim, C. M. Kim, S. H. Kim and B. S. Chung, *Biochem Biophys Res. Commun.* **1996**, *221*, 95-100.
- [25] A. M. Brouwer, *Pure. Appl. Chem.* **2011**, *83*, 2213-2228.
- [26] M. Frisch, G. Trucks, H. Schlegel, G. Scuseria, M. Robb, J. Cheeseman, G. Scalmani, V. Barone, B. Mennucci and G. Petersson, Wallingford, CT **2009**, *32*, 5648-5652.

FULL PAPER

Entry for the Table of Contents



We report a general and simple approach to synthesize Si-rhodamines bearing various functional substituents and application for monitoring the temperature change of mitochondrial.